

Wideband Communication with High-Dimensional Arrays: New Results and Transceiver Architectures

John H. Brady and Akbar M. Sayeed
Electrical and Computer Engineering
University of Wisconsin - Madison
Madison, WI, USA

Abstract—Wideband high-dimensional antenna arrays are expected to play a key role in future 5G wireless systems. Due to narrow beamwidths, phased array/beamforming methods are the natural choice for design and analysis of high-dimensional MIMO systems. However, conventional methods are based on the narrowband assumption which is violated as the bandwidth and array dimension increase. In this paper we revisit the use of high-dimensional arrays in line-of-sight single-input multiple-output (SIMO) systems. We develop a channel model that reveals coupling between the spatial and temporal dimensions that is not captured by conventional separable models. We then apply beamspace MIMO (B-MIMO) theory - system representation with respect to orthogonal spatial beams - to analyze system performance. Our analysis reveals a key dispersion factor Δ_{ch} that captures the impact of array dimension and bandwidth on performance. We show that Δ_{ch} characterizes the magnitude of the coupled signal dispersion in spatial angle and time. This leads to new B-SIMO transceivers that use on the order of Δ_{ch} beams to deliver near-optimal performance with dramatically low complexity compared to the optimal receiver. We present results that demonstrate the significant losses incurred by phased array receivers, and the near-optimal performance of low-complexity B-SIMO transceivers. Extension of the new wideband LoS SIMO model to MISO, MIMO, and multipath scenarios is outlined.

Index Terms—beamforming, millimeter-wave, high-dimensional MIMO, massive MIMO, wideband MIMO

I. INTRODUCTION

Capacity demands on wireless networks are rapidly increasing with the proliferation of data intensive wireless devices. Wideband, high-dimensional antenna arrays are expected to be a key technology for enabling high data rates and network functionality in 5G. In particular, millimeter-wave (mm-wave) systems operating from 30-300 GHz are a natural setting for wideband high-dimensional multiple-input multiple-output (MIMO) operation through orders-of-magnitude larger bandwidths and small wavelengths. The large number of MIMO degrees of freedom can be exploited for a number of critical capabilities, including [1]–[4]: higher antenna/beamforming gain; higher spatial multiplexing gain; and highly directional communication with narrow beams.

Due to narrow beamwidths, wireless channels induced via high-dimensional arrays are dominated by line-of-sight (LoS) and sparse multipath propagation. This motivates the use of phased array/beamforming models for system analysis [1], [2], [5]–[9] and analog beamforming transceiver architectures based on phased arrays [8] and lens arrays [1], [5]. However these models are based on a narrowband assumption, which is violated as the bandwidth and array dimension increase.

This work is partly supported by the NSF under grants ECCS-1247583 and IIP-1444962, and the Wisconsin Alumni Research Foundation.

This leads to beam squint [10], i.e. beams changing direction with frequency. While current systems using relatively small arrays and sub-bands of the available bandwidth can use beamforming designed for each sub-band to mitigate this problem [11], this solution does not scale. Traditionally, true time delay beamforming [12], [13] that replicates this frequency dependent beam angle has been used to solve this problem. However, the high dimension of mm-wave arrays makes digital implementation impractical and presents significant challenges to scaling up the dimension of analog true time delay beamformers (e.g. [14], [15]).

In this paper we consider wideband LoS single-input multiple-output (SIMO) communication induced by a uniform linear array (ULA) of antennas at the receiver. We develop a channel model that reveals the coupling between the spatial and temporal dimensions that is not captured by separable narrowband models. We then apply the concept of beamspace MIMO (B-MIMO) – system representation with respect to orthogonal spatial beams – to analyze system performance and develop new transceiver architectures. This analysis reveals a key channel dispersion parameter Δ_{ch} that quantifies the impact of the array dimension and bandwidth on the magnitude of the dispersion in space and time. Additionally Δ_{ch} represents the number of orthogonal beams needed to capture the effect of beam squint over the bandwidth of interest. This leads to new B-SIMO receiver architectures that sample a small number of orthogonal beams on the order of Δ_{ch} to deliver near optimal performance with dramatically reduced complexity compared to the optimum receiver that we characterize (and show to correspond to true time delay beamforming). Analytical and numerical performance results are presented that demonstrate the significant losses incurred by phased array based receivers even at relatively narrow bandwidths, and the flexibility of the low-complexity B-SIMO receiver to optimize the performance-complexity tradeoff inherent to high-dimensional systems. Finally, we outline the extension of the wideband LoS SIMO model to MISO, SIMO and multipath scenarios. **Notation:** \mathbf{x} is a vector; \mathbf{X} is a matrix; $\underline{\mathbf{x}}(t)$ is a vector valued function of time with Fourier transform $\underline{\mathbf{X}}(f) = \mathcal{F}\{\underline{\mathbf{x}}(t)\} = \int \underline{\mathbf{x}}(t)e^{-j2\pi ft} dt$.

II. SIMO LINE-OF-SIGHT SYSTEM

Consider SIMO communication between a single antenna transmitter and an M -dimensional ULA receiver operating at a carrier frequency f_c . The two-sided signal bandwidth is $W = \alpha f_c$, $\alpha \in (0, 2]$, where α is the fractional bandwidth; typically $\alpha \ll 1$. The transmitter sends a signal $s(t)$ of duration T that belongs to a signal space of dimension $N \approx TW$.

A. Antenna Domain and BeamSpace Representations

As we show in Sec. II-B, in contrast with separable phased array based models, the M -dimensional complex baseband signal received at the antenna array $\underline{r}(t)$ is related to $s(t)$ via

$$\underline{r}(t) = (\underline{h} \star s)(t) + \underline{w}(t); \underline{R}(f) = \underline{H}(f)S(f) + \underline{W}(f) \quad (1)$$

where $\underline{h}(\tau)$ is the $M \times 1$ spatial channel impulse response, $\underline{H}(f) = \mathcal{F}\{\underline{h}(\tau)\}$ is the spatial frequency response, and $\underline{w}(t)$ is a spatially and temporally white complex additive white Gaussian noise with power spectral density N_o .

The beamSpace channel representations in time and frequency are obtained by projecting the signal onto a set of orthonormal array steering vectors (beams) at the receiver [1], [16]. The steering vector $\mathbf{a}_M(\theta)$ is defined as

$$\mathbf{a}_M(\theta) = [e^{-j2\pi k\theta}]_{k \in \mathcal{I}(M)} \quad (2)$$

where $\mathcal{I}(M) = \{\ell - \frac{M-1}{2} : \ell = 0, \dots, M-1\}$ is a symmetric set of indices centered around 0. The columns of the beamforming matrix, \mathbf{U}_M , are steering vectors corresponding to M fixed spatial angles with uniform spacing $\Delta\theta = \frac{1}{M}$

$$\mathbf{U}_M = \frac{1}{\sqrt{M}} [\mathbf{a}_M(i\Delta\theta)]_{i \in \mathcal{I}(M)} \quad (3)$$

that represent M orthogonal beams forming a basis for the M -dimensional spatial signal space. In fact, \mathbf{U}_M is a unitary discrete Fourier transform (DFT) matrix $\mathbf{U}_M^H \mathbf{U}_M = \mathbf{U}_M \mathbf{U}_M^H = \mathbf{I}_M$. The beamSpace system models in time and frequency are

$$\underline{r}_b(t) = \mathbf{U}_M^H \underline{r}(t) = (\underline{h}_b \star s)(t) + \underline{w}_b(t) \quad (4)$$

$$\underline{R}_b(f) = \mathbf{U}_M^H \underline{R}(f) = \underline{H}_b(f)S(f) + \underline{W}_b(f) \quad (5)$$

where the beamSpace channel impulse response and the beamSpace channel frequency response are given by

$$\underline{h}_b(\tau) = \mathbf{U}_M^H \underline{h}(\tau), \quad \underline{H}_b(f) = \mathbf{U}_M^H \underline{H}(f). \quad (6)$$

B. Wideband Line-of-Sight SIMO Channel Model

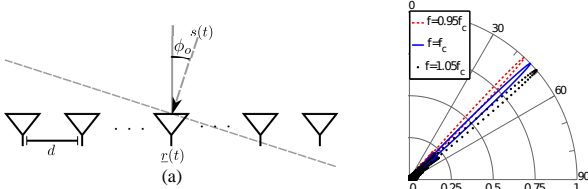


Fig. 1: (a) LoS SIMO System. (b) Far-field beam patterns induced by a fixed steering vector at three frequencies.

We consider a channel induced by LoS propagation between a point source located in the far field at an angle of $\phi_o \in [-\pi/2, \pi/2]$ and an M -dimensional ULA as shown in Fig. 1. We consider half-wavelength spacing at f_c : $d = \lambda_c/2$. The signal arrives at each array element with a slightly different delay. Assuming without loss of generality that the delay is 0 at the array center, the delay at the k^{th} element is

$$\tau_k = k\delta\tau, \quad k \in \mathcal{I}(M); \quad \delta\tau = \frac{d}{c} \sin(\phi_o), \quad d = \lambda_c/2 \quad (7)$$

where $\delta\tau$ is the delay between adjacent elements. Down mixing the signal from f_c , also manifests the delay as a phase shift between array elements, $2\pi\theta_k = 2\pi k\theta_o$, determined by the normalized spatial (beam) angle at the carrier frequency:

$$\theta_o = \delta\tau f_c = \frac{d}{\lambda_c} \sin(\phi_o). \quad (8)$$

In narrowband systems the effects of the delay on $s(t)$ can be ignored resulting in the baseband phased array model:

$$\underline{r}(t) = \mathbf{a}_M(\theta_o)s(t) + \underline{w}(t); \quad \underline{h}(\tau) = \mathbf{a}_M(\theta_o)\delta(\tau). \quad (9)$$

As the array dimension and bandwidth increase this is not true and the baseband channel spatial impulse response is

$$\underline{h}(\tau) = [h_k(\tau)]_k; \quad h_k(\tau) = e^{-j2\pi k\theta_o} W \text{sinc}(W(\tau - k\delta\tau)) \quad (10)$$

where $k \in \mathcal{I}(M)$ and bandlimitation leads to the sinc(\cdot) function. The k^{th} element of the spatial frequency response is

$$H_k(f) = \mathcal{F}\{h_k(\tau)\} = e^{-j2\pi k(\delta\tau f + \theta_o)}, \quad (11)$$

and from (2), (8), and (11) the channel's spatial frequency response in the general case is

$$\underline{H}(f) = \mathbf{a}_M(\theta(f)), \quad -W/2 \leq f \leq W/2 \quad (12)$$

with frequency dependent spatial angle

$$\theta(f) = \theta_o \left(\frac{f}{f_c} + 1 \right), \quad -W/2 \leq f \leq W/2. \quad (13)$$

Thus, a point source in a fixed direction ϕ_o will induce different beam angles $\theta(f)$ at different frequencies. Conversely, a fixed beam steering vector, like $\mathbf{a}_M(\theta_o)$ in (9) in a traditional phased array and calibrated to $\phi_o \leftrightarrow \theta_o$ at $f = f_c$ via (8), will focus power in different physical directions at different frequencies defined by $\theta(f)$ in (13) and obtained by inverting (8) at a given f : $\phi(f) = \sin^{-1}(\theta(f) * 2\lambda/\lambda_c)$. Fig. 1(b) illustrates this beam squinting by plotting the far-field beam-pattern $|\mathbf{a}_M(\theta_o)^H \mathbf{a}_M(\theta(f))|^2$, induced by a fixed steering vector aimed at $\phi_o = 55^\circ \leftrightarrow \theta_o = 0.41$, at three different frequencies: $f_c, (1 \pm 0.05)f_c$.

The beamSpace channel impulse response is

$$\underline{h}_b(\tau) = \mathbf{U}_M^H \underline{h}(\tau) = [h_{b,i}(\tau)]_{i \in \mathcal{I}(M)} \quad (14)$$

$$h_{b,i}(\tau) = \frac{1}{\sqrt{M}} \sum_{k \in \mathcal{I}(M)} e^{-j2\pi k(\theta_o - i\Delta\theta)} W \text{sinc}(W(\tau - k\delta\tau)),$$

and the beamSpace channel frequency response is

$$\underline{H}_b(f) = \mathbf{U}_M^H \underline{H}(f) = [H_{b,i}(f)]_{i \in \mathcal{I}(M)} \quad (15)$$

$$H_{b,i}(f) = \frac{1}{\sqrt{M}} \mathbf{a}_M^H(i\Delta\theta) \underline{H}(f) = \frac{1}{\sqrt{M}} D_M(\theta(f) - i\Delta\theta).$$

Here $D_M(\theta) = \frac{\sin(\pi M\theta)}{\sin(\pi\theta)}$ is the Dirichlet sinc function with $D_M(0) = M$ and $D_M(m\Delta\theta) = 0$ for integers $m \neq 0$.

C. Channel Dispersion Factor

While the phased array model (9) shows no dispersion in spatial angle or time, (10) and (12) show dispersion in time across the aperture and dispersion in spatial angle across the bandwidth. Thus a point source in narrowband systems spreads across spatial angle and time in wideband, high dimensional systems. As we show, if this dispersion is not accounted for it leads to severe power loss and pulse distortion. The magnitude of this dispersion is determined by how many resolvable beams and delays the LoS channel occupies [17]. The angular spread of the channel over the bandwidth is

$$\Delta\theta_{ch} = |\theta(W/2) - \theta(-W/2)| = \alpha|\theta_o|. \quad (16)$$

Dividing this by the orthogonal beam spacing $\Delta\theta = \frac{1}{M}$ yields

$$\Delta\theta_{ch}/\Delta\theta = M\alpha|\theta_o|, \quad (17)$$

the number of orthogonal beams spanned by the spatial dispersion. Similarly, the delay spread across the aperture is

$$\Delta\tau_{ch} = M|\delta\tau|, \quad (18)$$

which divided by delay resolution $\Delta\tau = \frac{1}{W}$ yields

$$\Delta\tau_{ch}/\Delta\tau = W\Delta\tau_{ch} = M\alpha|\theta_o|, \quad (19)$$

the number of resolvable delays spanned by the delay dispersion. Thus, this *channel dispersion factor*

$$\Delta_{ch} = M\alpha|\theta_o| = \Delta\tau_{ch}/\Delta\tau = \Delta\theta_{ch}/\Delta\theta \quad (20)$$

characterizes the spreading of a LoS path in both angle and delay. For transmitters located at $\phi_o = 0 \leftrightarrow \theta_o = 0$, $\Delta_{ch} = 0$ and no dispersion occurs. However for any $\phi_o \neq 0 \leftrightarrow \theta_o \neq 0$, there is dispersion, and its magnitude increases as the bandwidth and array dimension increase.

III. RECEIVER ARCHITECTURES FOR LOS SIMO SYSTEMS

Consider a transmitted signal of the form [17]:

$$s(t) = \sum_{\ell=0}^{N-1} s_{\ell}\psi_{\ell}(t); \quad S(f) = \sum_{\ell=0}^{N-1} s_{\ell}\Psi_{\ell}(f) \quad (21)$$

where the $\{s_{\ell}\}_{\ell=0}^{N-1}$ are the independent information symbols with energy $E[|s_{\ell}|^2] = \mathcal{E}_s$ and the $\{\psi_{\ell}(t)\}_{\ell=0}^{N-1}$ form an orthonormal basis for the $N \approx TW$ dimensional signal space. The sufficient statistics $\{z_{\ell}\}_{\ell=0}^{N-1}$ for detecting the information symbols $\{s_{\ell}\}$ are obtained by taking the inner product of the received signal with waveforms $\{\underline{g}_{\ell}(t)\}_{\ell=0}^{N-1}$ representing a mapping of $\{\psi_{\ell}(t)\}_{\ell=0}^{N-1}$ into the spatio-temporal receive signal space. The inner product is

$$\langle \underline{x}, \underline{y} \rangle = \int \underline{y}^H(t)\underline{x}(t)dt = \int \underline{Y}^H(f)\underline{X}(f)df \quad (22)$$

with the associated norm $\|\underline{x}\|^2 = \langle \underline{x}, \underline{x} \rangle$. This inner product may be calculated in either the spatial domain or beamspace, and in time or frequency. Thus the z_{ℓ} are given by

$$\begin{aligned} z_{\ell} = \langle \underline{r}, \underline{g}_{\ell} \rangle &= \sum_{\ell'=0}^{N-1} s_{\ell'} \langle (\underline{h} * \psi_{\ell'}), \underline{g}_{\ell} \rangle + \langle \underline{w}, \underline{g}_{\ell} \rangle \\ &= s_{\ell}A_{\ell} + \sum_{\ell' \neq \ell} s_{\ell'}B_{\ell, \ell'} + W_{\ell}. \end{aligned} \quad (23)$$

where the signal amplitude and interference are

$$A_{\ell} = \langle (\underline{h} * \psi_{\ell}), \underline{g}_{\ell} \rangle, \quad B_{\ell, \ell'} = \langle (\underline{h} * \psi_{\ell'}), \underline{g}_{\ell} \rangle \quad (24)$$

and $W_{\ell} \sim \mathcal{CN}(0, N_o\|\underline{g}_{\ell}\|^2)$ represents the noise. For a given choice of basis functions $\{\psi_{\ell}(t)\}$ the signal to interference and noise (SINR) for the ℓ^{th} test statistic (z_{ℓ}) is

$$\text{SINR}_{\ell} = \frac{\frac{\mathcal{E}_s}{N_o}|A_{\ell}|^2}{\sum_{\ell' \neq \ell} |B_{\ell, \ell'}|^2 + \|\underline{g}_{\ell}\|^2} \quad (25)$$

In the limit of low SNR ($\frac{\mathcal{E}_s}{N_o} \rightarrow 0$) and high SNR ($\frac{\mathcal{E}_s}{N_o} \rightarrow \infty$),

$$\text{SINR}_{\ell} \rightarrow \frac{E_s}{N_o} \frac{|A_{\ell}|^2}{\|\underline{g}_{\ell}\|^2}, \quad \text{SINR}_{\ell} \rightarrow \frac{|A_{\ell}|^2}{\sum_{\ell' \neq \ell} |B_{\ell, \ell'}|^2}. \quad (26)$$

A. Optimal Matched Filter Receiver

The natural choice for $\underline{g}_{\ell}(t)$ is the matched filter

$$\underline{g}_{\ell}(t) = \frac{1}{\sqrt{M}}(\underline{h} * \psi_{\ell})(t); \quad \underline{G}_{\ell}(f) = \frac{1}{\sqrt{M}}H(f)\Psi_{\ell}(f) \quad (27)$$

with norm $\|\underline{g}_{\ell}\|^2 = 1$. This results in signal amplitude

$$A_{\ell} = \frac{1}{\sqrt{M}} \int_{-\frac{W}{2}}^{\frac{W}{2}} \Psi_{\ell}^*(f) \mathbf{a}_M^H(\theta(f)) \mathbf{a}_M(\theta(f)) \Psi_{\ell}(f) df = \sqrt{M} \quad (28)$$

and interference

$$B_{\ell, \ell'} = \frac{1}{\sqrt{M}} \int_{-\frac{W}{2}}^{\frac{W}{2}} \Psi_{\ell}^*(f) \mathbf{a}_M^H(\theta(f)) \mathbf{a}_M(\theta(f)) \Psi_{\ell'}(f) df = 0. \quad (29)$$

Thus the matched filter introduces no interference regardless of the choice of basis functions and the SINR is the signal-to-noise ratio (SNR) and is the same for all z_{ℓ} :

$$\text{SINR}_{\ell} = \text{SNR}_{\ell} = M \frac{\mathcal{E}_s}{N_o}. \quad (30)$$

Plugging (27) into (23) yields

$$z_{\ell} = \int \underline{g}_{\ell}^H(t)\underline{r}(t)dt = \int \psi_{\ell}^*(\tau) \left[\int \underline{h}^H(t-\tau)\underline{r}(t)dt \right] d\tau \quad (31)$$

So the optimal receiver can be interpreted as a bank of M adjustable delay filters and phase shifters defined by $h_k(\tau)$ followed by spatial combining, and then correlation with the basis functions as shown in Fig. 2(a). Note that this space-time processing corresponds to true time delay beamforming [12].

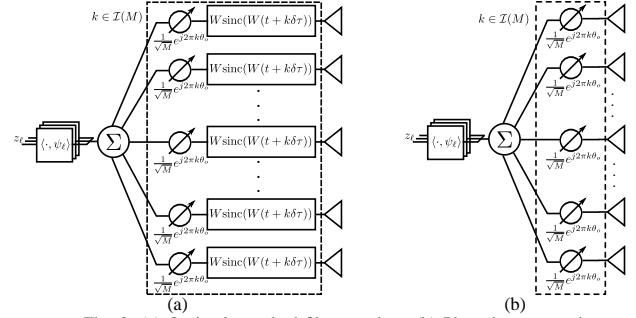


Fig. 2: (a) Optimal matched-filter receiver. (b) Phased-array receiver.

B. Phased Array Receiver

For the phased array receiver $\underline{g}_{\ell}(t)$ is given by

$$\underline{g}_{\ell}(t) = \frac{1}{\sqrt{M}} \mathbf{a}_M(\theta_o) \psi_{\ell}(t) \quad (32)$$

with norm $\|\underline{g}_{\ell}\|^2 = 1$ which corrects for the phase shift across the antenna elements in (10) but does not perform any temporal equalization to account for the delays. This results in the following signal amplitude and interference terms

$$\begin{aligned} A_{\ell} &= \frac{1}{\sqrt{M}} \int_{-\frac{W}{2}}^{\frac{W}{2}} \Psi_{\ell}^*(f) \mathbf{a}_M^H(\theta_o) \mathbf{a}_M(\theta(f)) \Psi_{\ell}(f) df \\ &= \frac{1}{\sqrt{M}} \int_{-\frac{W}{2}}^{\frac{W}{2}} |\Psi_{\ell}(f)|^2 D_M \left(\theta_o \frac{f}{f_c} \right) df \end{aligned} \quad (33)$$

$$B_{\ell, \ell'} = \frac{1}{\sqrt{M}} \int_{-\frac{W}{2}}^{\frac{W}{2}} \Psi_{\ell}^*(f) D_M \left(\theta_o \frac{f}{f_c} \right) \Psi_{\ell'}(f) df. \quad (34)$$

In contrast with the matched filter, the SINR of the phased array receiver depends on Δ_{ch} and the choice of basis functions. As shown in Fig. 4(c) in Sec. IV-A, as Δ_{ch} increases, $D_M(\theta_o \frac{f}{f_c})$ varies significantly over the bandwidth; this results in power loss from (33) and interference between basis functions from (34).

The phased array receiver is shown in Fig. 2(b) and cor-

responds to removing the filter bank used for space-time equalization in the optimal receiver in Fig. 2(a). In the special case when $\theta_o = i_o \Delta\theta$, the phased-array is a special case of the beamspace receiver in which only the i_o^{th} beam is used.

C. Low-Complexity Near Optimal Beamspace Receiver

The optimal matched filter receiver (27) in beamspace is

$$\underline{g}_{b,\ell}(t) = \frac{1}{\sqrt{M}}(\underline{h}_b * \psi_\ell)(t); \underline{G}_{b,\ell}(f) = \frac{1}{\sqrt{M}}\underline{H}_b(f)\Psi_\ell(f) \quad (35)$$

with norm 1, which operates on $\underline{r}_b(t) = \mathbf{U}_M^H \underline{r}(t)$ and performs space-time equalization over all M beams. The signal and interference terms are identical to the optimum receiver

$$A_\ell = \frac{1}{\sqrt{M}} \int_{-\frac{W}{2}}^{\frac{W}{2}} |\Psi_\ell(f)|^2 \underline{H}_b^H(f) \underline{H}_b(f) df = M \quad (36)$$

$$B_{\ell,\ell'} = \frac{1}{\sqrt{M}} \int_{-\frac{W}{2}}^{\frac{W}{2}} \Psi_\ell^*(f) \underline{H}_b^H(f) \underline{H}_b(f) \Psi_{\ell'}(f) df = 0, \quad (37)$$

which follow from the following equivalent relations for the aggregate channel power spectral density (PSD):

$$\|\underline{H}(f)\|^2 = \underline{H}^H(f) \underline{H}(f) = \sum_{k \in \mathcal{I}(M)} |H_k(f)|^2 = M$$

$$\|\underline{H}_b(f)\|^2 = \underline{H}_b^H(f) \underline{H}_b(f) = \sum_{i \in \mathcal{I}(M)} |H_{b,i}(f)|^2 = M \quad (38)$$

where $|H_k(f)|^2 = 1$ is the PSD for the k -th antenna, and $S_{b,i}(f) = |H_{b,i}(f)|^2 = \frac{1}{M} D_M^2(\theta(f) - i\Delta\theta)$ is the PSD for the i^{th} beam. The above relation states that aggregate PSD is flat in both the antenna domain and the beamspace domain. However, while the PSD for each antenna is also flat, the PSDs for different beams are localized and each beam captures part of the flat aggregate PSD as illustrated in Fig. 4. Furthermore, as discussed in Sec. IV-A and illustrated in Fig. 5, for a given value of Δ_{ch} , approximately Δ_{ch} beams are needed to capture most of the aggregate flat PSD over the bandwidth of interest.

This suggests an approach for designing low-complexity beamspace receivers that deliver near-optimal performance. Define the total channel power as

$$\begin{aligned} \sigma^2 &= \frac{1}{W} \int_{-\frac{W}{2}}^{\frac{W}{2}} \underline{H}_b^H(f) \underline{H}_b(f) df = \sum_{i \in \mathcal{I}(M)} \sigma_i^2 = M \\ \sigma_i^2 &= \frac{1}{W} \int_{-\frac{W}{2}}^{\frac{W}{2}} S_{b,i}(f) df = \frac{1}{W} \int_{-\frac{W}{2}}^{\frac{W}{2}} |H_{b,i}(f)|^2 df \quad (39) \end{aligned}$$

where σ_i^2 is the power in the i^{th} beam. Since the majority of the power is captured by approximately Δ_{ch} beams, a low-complexity B-SIMO receiver can be designed by processing only this set of dominant beams defined as:

$$\mathcal{M} = \{i \in \mathcal{I}(M) : \sigma_i^2 \geq \gamma \sigma^2\} \quad (40)$$

Then if the threshold $\gamma \in (0, 1)$ is chosen properly, $p = |\mathcal{M}| \approx \Delta_{ch}$, and the beams in \mathcal{M} will result in an approximately flat aggregate PSD; see (38) and Fig. 5. The near-optimal B-SIMO receiver is defined by

$$g_{b,\ell,i}(t) = \begin{cases} \frac{1}{\sqrt{M}}(h_{b,i} * \psi_\ell)(t) & i \in \mathcal{M} \\ 0 & i \notin \mathcal{M} \end{cases} \quad (41)$$

with norm $\|g_{b,\ell}\|^2 = \frac{1}{M^2} \int |\Psi_\ell(f)|^2 \left(\sum_{i \in \mathcal{M}} D_M^2(\theta(f) - i\Delta\theta) \right) df$.

This gives the following signal and interference terms

$$A_\ell = \frac{1}{M^{\frac{3}{2}}} \int_{-\frac{W}{2}}^{\frac{W}{2}} |\Psi_\ell(f)|^2 \left(\sum_{i \in \mathcal{M}} D_M^2(\theta(f) - i\Delta\theta) \right) df \quad (42)$$

$$B_{\ell,\ell'} = \frac{1}{M^{\frac{3}{2}}} \int_{-\frac{W}{2}}^{\frac{W}{2}} \Psi_\ell^*(f) \left(\sum_{i \in \mathcal{M}} D_M^2(\theta(f) - i\Delta\theta) \right) \Psi_{\ell'}(f) df. \quad (43)$$

As shown in Fig. 5, when $p \approx \Delta_{ch}$, $\sum_{i \in \mathcal{M}} \frac{1}{M} D_M^2(\theta(f) - i\Delta\theta) \approx M$ over the bandwidth, yielding $A_\ell \approx \sqrt{M}$ and $B_\ell \approx 0$. So in contrast with the phased array receiver, by performing space-time filtering over $p \approx \Delta_{ch}$ beams, the low-complexity B-SIMO receiver is able to attain near-optimum performance.

The full-complexity implementation of the beamspace receiver is shown in Fig. 3(a), which is also equivalent to the optimal receiver in Fig. 2(a). A bank of M filters defined by $\underline{h}_{b,i}(\tau)$ is applied to each beam (after the transformation into beamspace through \mathbf{U}_M) before combining and correlation. The low-complexity near-optimal configuration is shown in Fig. 3(b) in which the filtering and combining is done over the dominant $p \approx \Delta_{ch}$ beams in \mathcal{M} . This results in a complexity reduction by a factor of $\alpha\theta_o$, compared to Fig. 3(a).

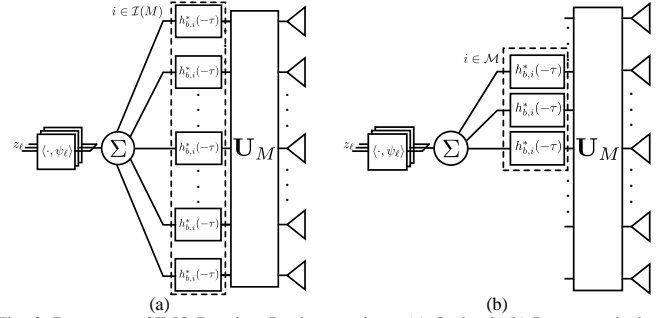


Fig. 3: Beamspace SIMO Receiver Implementations: (a) Optimal, (b) Low-complexity.

IV. NUMERICAL RESULTS

In this section we first present numerical results that illustrate the effects of dispersion in the wideband channel and how the B-SIMO receiver mitigates this dispersion by processing the $p = |\mathcal{M}|$ dominant beams. We then give results that compare the receivers' performance for both single-carrier and orthogonal frequency division multiplexing (OFDM) waveforms. All the results are calculated for a $M = 61$ element, $\frac{\lambda_c}{2}$ spaced array (6" array at 60 GHz) receiving a signal from a transmitter located at $\phi_o = 55^\circ \leftrightarrow \theta_o = 0.41$ corresponding to the $i_o = 25$ -th beam in the B-SIMO receiver; i.e., $\theta_o = 25\Delta\theta$.

A. Dispersion Effects: Power Loss and Interference

Inspecting the expressions for the A_ℓ and $B_{\ell,\ell'}$ for different receivers, we note that they are governed by an effective channel frequency response $E(f)$ given by

$$E_{opt}(f) = M, \quad E_{pa}(f) = D_M(\theta_o f / f_c), \quad E_b(f) = \sum_{i \in \mathcal{M}} S_{b,i}(f)$$

$E_{opt}(f)$ is flat and thus the optimum receiver captures all signal power for all basis functions and there is no inference. This is also true for the beamspace receiver which uses all beams.

From (13) and (15), $S_{b,i}(f) = \frac{1}{M} D_M^2 \left(\theta_o \frac{f}{f_c} + (i_o - i)\Delta\theta \right)$. Fig. 4 plots $S_{b,i}(f)$ as a function of normalized frequency for 5 values of i centered on $i_o = 25$. In particular, $S_{b,i_o}(f) = |a_M^H(\theta_o) \underline{H}(f)|^2 = \frac{1}{M} D_M^2(\theta_o \frac{f}{f_c})$, shown in Fig. 4(c), also

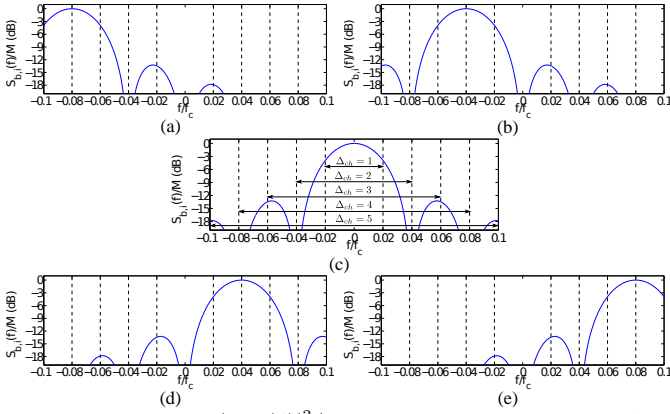


Fig. 4: Normalized plots of $|H_{b,i}(f)|^2/M$ for an $M = 61$ element array with $\theta_o = 25\Delta\theta_o$ for (a) $i = 23$, (b) $i = 24$, (c) $i = i_o = 25$, (d) $i = 26$, and (e) $i = 27$.

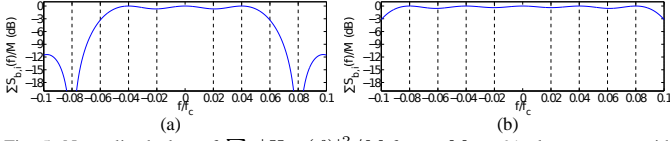


Fig. 5: Normalized plots of $\sum_i |H_{b,i}(f)|^2/M$ for an $M = 61$ element array with $\theta_o = 25\Delta\theta_o$ for (a) $i \in \{24, 25, 26\}$ and (b) $i \in \{23, 24, 25, 26, 27\}$

reflects the PSD of the phased-array effective response $E_{pa}(f)$. When $\Delta_{ch} \ll 1$ ($|f/f_c| \ll 0.02$ over the bandwidth), $S_{b,i_o}(f) \approx M$ and $S_{b,i \neq i_o}(f) \approx 0$. So both phased array receiver and the B-SIMO receiver will exhibit no power loss or interference. Increasing Δ_{ch} causes variation in $S_{b,i_o}(f)$. In particular for $\Delta_{ch} = 2$ ($|f/f_c| \leq 0.04$) nulls begin to appear in $S_{b,i_o}(f)$. Thus for $\Delta_{ch} \geq 1$ using a phased array receiver results in power loss and interference, which gets more severe for larger Δ_{ch} . On the other hand, it is clear from Fig. 4 that the power lost in $S_{b,i_o}(f)$ is present in the adjacent beams. As shown in Fig. 5(a) for $\Delta_{ch} \leq 3$ ($|f/f_c| \leq 0.06$), combining the three beams centered on i_o (Fig. 4(b)-(d)) results in an approximately flat effective $E_b(f)$ (see also (38)). If Δ_{ch} is increased to 5 ($|f/f_c| \leq 0.1$), 3 beams are no longer sufficient but using all the 5 beams shown in Fig. 4 results in a flat effective $E_b(f)$ as shown in Fig. 5(b). In general, for a given Δ_{ch} , a B-SIMO receiver with $p = |\mathcal{M}| \approx \Delta_{ch}$ dominant beams (see (41)) is needed for near-optimal performance.

B. SIMO Receiver Performance Comparison

This section compares the performance of phased array and B-SIMO receivers. First SINR results are presented for single carrier systems where the N basis functions are delayed versions of the sinc pulse of bandwidth W : $\psi_\ell(t) = W \text{sinc}(W(t - \ell/W))$. The signal power $|A_\ell|^2$ is constant and the interference power $|B_{\ell,\ell'}|^2$ is completely determined by $|\ell - \ell'|$. For the values of α considered $|B_{\ell,\ell'}|^2$ drops below -40 dB of the maximum for $|\ell - \ell'| > 8$. Thus the numerical SINR results, calculated for the central $\lceil \frac{N}{2} \rceil^{\text{th}}$ pulse, provide a good assessment of the SINR of any pulse for $N > 16$, except for edge cases where interference will be at most 3 dB lower. For the OFDM simulations, we assume that the signal duration T is sufficiently long so that there is no interference ($B_{\ell,\ell'} \approx 0$). The spectral efficiency is calculated by performing waterfilling over the subcarriers with the SNR for each calculated via (25).

Fig. 6(a)-(c) plots the single carrier SINR of the different receivers as a function of $\frac{E_s}{N_o}$ for several values of α (Δ_{ch}). As expected, Fig. 6(a) shows severe performance loss for the

phased array receiver as α (Δ_{ch}) increases. For all but the smallest value of α , the receiver suffers from interference and for $\alpha \geq 0.08$ ($\Delta_{ch} \geq 2$) this is compounded by severe power loss due to nulls in $D_M(\theta_o \frac{f}{f_c})$ over the bandwidth (see Fig. 4(c)). On the other hand, the SINR of the 3-beam and 5-beam B-SIMO receivers shown in 6(b) and (c), respectively, exhibit significantly reduced interference, and essentially no power loss when $p = |\mathcal{M}| \geq \Delta_{ch}$. Finally, Fig. 6(d) shows the spectral efficiency of the phased array and near-optimal B-SIMO receivers. The plots for $\alpha = 0.02$ ($\Delta_{ch} = 0.5$) show that OFDM eliminates the performance loss due to interference in the phased array receiver for smaller values of Δ_{ch} . However, the plots for $\alpha = 0.12$ and 0.2 ($\Delta_{ch} = 3$ and 5) show that the power loss in the phased array receiver for $\Delta_{ch} \geq 2$ results in severe and unavoidable performance loss. In comparison, the B-SIMO receivers ($p = 1, 3, 5$ beams for $\Delta_{ch} = 0.5, 3, 5$) suffer from nearly no power loss or interference. These results demonstrate the near-optimum performance of B-SIMO receiver with sufficiently large number of beams $p = |\mathcal{M}| \geq \Delta_{ch}$.

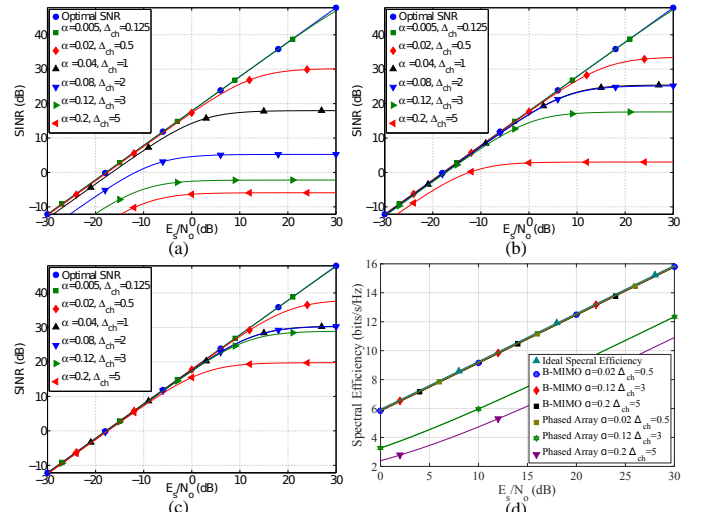


Fig. 6: Plots of the single-carrier receiver SINR as a function of E_s/N_o for the LoS SIMO channel: (a) the phased array receiver, and the near-optimal beamspace receiver with (b) 3 beams and (c) 5 beams. (d): OFDM spectral efficiency of the phased array and near-optimal beamspace receivers for the same LoS SIMO channel.

V. EXTENSIONS: MISO, MIMO AND MULTIPATH

We briefly discuss extensions of the new wideband SIMO system model developed in Sec. II to MISO, MIMO, and multipath channels. Consider a MISO system with an M_T -element ULA transmitter communicating with a single-antenna receiver located at $\phi_{T,o} \leftrightarrow \theta_{T,o}$; see (8). The LoS wideband MISO system model (baseband frequency domain) is

$$R(f) = \underline{H}^H(f) \underline{X}(f) + W(f); \quad \underline{H}(f) = \mathbf{a}_{M_T}(\theta_T(f)) \quad (44)$$

where $R(f)$ is received signal, $\underline{X}(f)$ is the transmitted signal vector, $W(f)$ is noise, and the frequency-dependent beam angle $\theta_T(f)$ is related to $\theta_{T,o}$ as in (13). The $M_R \times M_T$ LoS MIMO model readily follows:

$$\underline{R}(f) = \mathbf{H}(f) \underline{X}(f) + \underline{W}(f); \quad \mathbf{H}(f) = \mathbf{a}_{M_R}(\theta_T(f)) \mathbf{a}_{M_T}^H(\theta_R(f))$$

where the LoS path with transmit/receive directions $(\phi_{T,o}, \phi_{R,o}) \leftrightarrow (\theta_{T,o}, \theta_{R,o})$ induces the frequency-dependent beam angles $(\theta_T(f), \theta_R(f))$ in the array steering vectors that define the channel frequency response matrix $\mathbf{H}(f)$. Finally,

the channel matrix for a wideband multipath MIMO channel can be modeled as

$$\mathbf{H}(f) = \sum_{\ell=1}^{N_p} \beta_{\ell} \mathbf{a}_{M_R}(\theta_{R,\ell}(f)) \mathbf{a}_{M_T}^H(\theta_{T,\ell}(f)) e^{-j2\pi\tau_{\ell}f} \quad (45)$$

where N_p denotes the number of paths, and the ℓ -th path is associated with a path gain β_{ℓ} , angle of departure $\phi_{T,\ell}$, angle of arrival $\phi_{R,\ell}$, and delay τ_{ℓ} . The physical angles $(\phi_{T,\ell}, \phi_{R,\ell}) \leftrightarrow (\theta_{T,\ell}, \theta_{R,\ell})$ induce frequency-dependent beam angles $(\theta_{T,\ell}(f), \theta_{R,\ell}(f))$ as in (13). The beamspace representation of $\mathbf{H}(f)$ is given by

$$\begin{aligned} \mathbf{H}_b(f) &= \mathbf{U}_{M_R}^H \mathbf{H}(f) \mathbf{U}_{M_T} = [H_{b,i,m}(f)]_{i \in \mathcal{I}(M_R), m \in \mathcal{I}(M_T)} \\ H_{b,i,m}(f) &= \sum_{\ell=1}^{N_p} \beta_{\ell} D_{M_R}(\theta_{R,\ell}(f) - i\Delta\theta_R) \\ &\quad D_{M_T}(\theta_{T,\ell}(f) - m\Delta\theta_T) e^{-j2\pi\tau_{\ell}f}, \end{aligned} \quad (46)$$

where $\Delta\theta_T = 1/M_T$ and $\Delta\theta_R = 1/M_R$ are the orthogonal beam spacings for the transmit and receive ULAs.

We note that conventional frequency-selective MIMO models (see, e.g., [17]) can be recovered from the above general wideband MIMO models by replacing the frequency-dependent transmit/receive beam angles for each path $(\theta_{T,\ell}(f), \theta_{R,\ell}(f))$ with their corresponding fixed values $(\theta_{T,\ell}, \theta_{R,\ell}) = (\theta_{T,\ell}(f), \theta_{R,\ell}(f))|_{f=0}$ defined at $f = f_c$ via (8). These conventional models also correspond to the phased array models discussed in the SIMO case. Similarly, we can define transmit/receive channel dispersion factors for each path: $\Delta_{ch,T,\ell} = M_T \alpha \theta_{T,\ell}$ and $\Delta_{ch,R,\ell} = M_R \alpha \theta_{R,\ell}$. The most important implication is that each path will be associated with a $\Delta_{ch,R,\ell}$ beams at the receiver and $\Delta_{ch,T,\ell}$ beams at the transmitter captured by a corresponding $\Delta_{ch,R,\ell} \times \Delta_{ch,T,\ell}$ sub-matrix of the beamspace matrix $\mathbf{H}_b(f)$. Low-complexity B-MIMO transceivers operate on these sub-matrices for each path to deliver near-optimal performance.

VI. CONCLUSIONS AND DISCUSSION

We have presented a study of wideband, high-dimensional SIMO systems for LoS channels. We developed a channel model that reveals the coupled signal dispersion in time and spatial angle and identified a key *channel dispersion factor* $\Delta_{ch} = M\alpha\theta_o$ that captures the magnitude of this dispersion as function of critical system parameters. In addition to characterizing the power loss and interference in phased array receivers, Δ_{ch} represents the number of dominant beams needed in the beamspace receivers to account for dispersion. This motivated the design of B-SIMO receivers that perform space-time processing only over these Δ_{ch} dominant beams resulting in dramatic complexity reduction. Our results showed the significant performance loss in phased array receivers even for relatively narrow bandwidths, and the near-optimum performance of the low-complexity B-MIMO receivers. Finally, we outlined extensions of the wideband LoS SIMO model to MISO, MIMO, and multipath that serve as guidelines for further research (e.g. multiuser MIMO).

The results of this paper are particularly relevant to mm-wave systems, where even current systems have encountered issues due to beam squint [11]. So if phased array based analog beamforming and larger bandwidths are used to im-

plement mm-wave transceiver architectures that utilize high dimensional arrays (e.g. [9]), performance loss will occur. However, the large array dimension makes recovering this lost performance via digital beamforming, e.g. using OFDM with a different digital beamformer for each subcarrier, impractical. Thus transceivers combining multi-beam B-MIMO processing with analog beamforming provide the best route for achieving the full performance in wideband, high dimensional mm-wave MIMO. In particular lens-based analog beamforming [1], [5] are a natural choice for such transceivers. Finally, although the results of this paper were derived for orthogonal waveforms, the concept of space-time processing over multiple orthogonal beams also applies to non-orthogonal waveforms, e.g. [18].

REFERENCES

- [1] A. M. Sayeed and N. Behdad, "Continuous Aperture Phased MIMO: Basic Theory and Applications," in *Proc. Allerton Conf.*, Sept. 29-Oct. 1 2010, pp. 1196–1203.
- [2] Z. Pi and F. Khan, "An Introduction to Millimeter-Wave Mobile Broadband Systems," *IEEE Comm. Mag.*, vol. 49, no. 6, pp. 101–107, June 2011.
- [3] T. L. Marzetta, "Noncooperative Cellular Wireless with Unlimited Numbers of Base Station Antennas," *IEEE Trans. Wireless Comm.*, vol. 9, no. 11, pp. 3590–3600, Nov. 2010.
- [4] T.S. Rappaport et. al., "Millimeter Wave Mobile Communications for 5G Cellular: It Will Work!," *IEEE Access*, vol. 1, pp. 335–349, 2013.
- [5] J. Brady, N. Behdad, and A.M. Sayeed, "Beamspace MIMO for Millimeter-Wave Communications: System Architecture, Modeling, Analysis, and Measurements," *IEEE Trans. Antennas and Propag.*, vol. 61, no. 7, pp. 3814–3827, July 2013.
- [6] A. Sayeed and J. Brady, "Beamspace MU-MIMO for High-Density Gigabit Small Cell Access at Millimeter-Wave Frequencies," in *SPAWC 2014*, June 2014, pp. 3785 – 3789.
- [7] V. Venkateswaran and A. van der Veen, "Analog Beamforming in MIMO Communications with Phase Shift Networks and Online Channel Estimation," *IEEE Trans. Signal Proc.*, vol. 58, no. 8, pp. 4131–4143, Aug. 2010.
- [8] O. El Ayach, R.W. Heath, S. Abu-Surra, S. Rajagopal, and Zhouyue Pi, "The Capacity Optimality of Beam Steering in Large Millimeter Wave MIMO Systems," in *SPAWC 2012*, June 2012, pp. 100–104.
- [9] A. Adhikary, E. Al Safadi, M.K. Samimi, Rui Wang, G. Caire, T.S. Rappaport, and A.F. Molisch, "Joint Spatial Division and Multiplexing for mm-Wave Channels," *IEEE J. Sel. Areas Commun.*, vol. 32, no. 6, pp. 1239–1255, June 2014.
- [10] R. J. Mailloux, *Phased Array Antenna Handbook*, Artech House, 2nd edition, 2005.
- [11] Zhijun Liu, W. ur Rehman, Xiaodong Xu, and Xiaofeng Tao, "Minimize Beam Squint Solutions for 60GHz Millimeter-Wave Communication System," in *Vehicular Technology Conference (VTC Fall), 2013 IEEE 78th*, Sept 2013, pp. 1–5.
- [12] H. Hashemi, Ta-Shun Chu, and J. Roderick, "Integrated true-time-delay-based ultra-wideband array processing," *IEEE Comm. Magazine*, vol. 46, no. 9, pp. 162–172, September 2008.
- [13] P. Moosbrugger, M. Adkins, and R. Haupt, "Degradation in theoretical phase shift keying waveforms due to signal dispersion in a large communications phased array," in *Phased Array Systems Technology, 2013 IEEE International Symposium on*, Oct 2013, pp. 224–226.
- [14] Ta-Shun Chu and H. Hashemi, "True-Time-Delay-Based Multi-Beam Arrays," *IEEE Trans. Microwave Theory and Tech.*, vol. 61, no. 8, pp. 3072–3082, Aug 2013.
- [15] T.P. McKenna, J.A. Nanzer, and T.R. Clark, "Photonic beamsteering of a millimeter-wave array with 10-gb/s data transmission," *IEEE Photon. Technol. Lett.*, vol. 26, no. 14, pp. 1407–1410, July 2014.
- [16] A. M. Sayeed, "Deconstructing Multiantenna Fading Channels," *IEEE Trans. Signal Proc.*, vol. 50, no. 10, pp. 2563–2579, Oct. 2002.
- [17] A. Sayeed and T. Sivanadyan, "Wireless Communication and Sensing in Multipath Environments with Multi-antenna Wireless Transceivers," in *Handbook on Array Procng and Sensor Networks 1st ed.*, K. J. R. Liu and S. Haykin, Eds., pp. 115–170. IEEE-Wiley, Hoboken, NJ, 2010.
- [18] G. Wunder et. al., "5GNOW: non-orthogonal, asynchronous waveforms for future mobile applications," *IEEE Comm. Mag.*, vol. 52, no. 2, pp. 97–105, February 2014.